Theoretical Physics

Dark Matter: Particle Evolution through Freeze-out

Dennis Alp
dalp@kth.se

Samuel Modée
smodee@kth.se

SA104X Degree Project in Engineering Physics, First Level
Department of Theoretical Physics
Royal Institute of Technology (KTH)
Supervisor: Tommy Ohlsson

May 21, 2014

Abstract

This report focuses on the evolution of dark matter particles in a simplified, homogeneous and isotropic model of the Universe. The purpose is to analyze theoretical predictions and recent experimental measurements to be able to draw conclusions about the properties of the dark matter particles. The inexperienced reader is introduced to the subject and thorough derivations of the formulas relevant to the analysis are made. To analyze the evolution of dark matter, the Boltzmann equation is applied to a freeze-out model. Both analytical and numerical approaches will be taken and discrepancies between those are investigated. Qualitative effects of the particle cross section and mass are studied and constraints on the parameters are set using experimental data. Finally, assumptions are discussed and suggestions for further research are made.

Sammanfattning

Rapporten fokuserar på utvecklingen av mörk materia-partiklar i en förenklad, homogen och isotrop modell av universum. Syftet är att analysera teoretiska förutsägelser och nyligen genomförda experimentella mätningar för att dra slutsatser om mörk materia-partiklarnas egenskaper. Den oerfarne läsaren introduceras till ämnet och en utförlig härledning av de relevanta formlerna genomförs. Boltzmannekvationen tillämpas på en utfrysningsmodell och används för att analysera utvecklingen av den mörka materian. Både analytiska och numeriska metoder används och skillnader mellan dessa studeras. Kvalitativa effekter av partiklarnas tvärsnitt och massa undersöks och begränsningar av parametrarna görs med hjälp av experimentell data. Slutligen diskuteras antaganden och förslag för fortsatt forskning läggs fram.

Contents

Chapter 1

Introduction

Ever since the early times of mankind, we have looked up at the night sky and tried to make sense of the apparent motion of the celestial bodies. The image of ourselves at the center of the Universe was shattered when Nicolaus Copernicus introduced the concept of heliocentrism [1]. From that time onward, it became increasingly clear that we are a very small part of an enormous universe.

Since then, our quest to describe the Universe has taken us past Johannes Kepler's laws for the elliptical orbits in the Solar System to Isaac Newton's theory of gravity which enables us to calculate the motions of many astronomical objects with great accuracy. However, events which were inexplicable by the prevailing theories of the time accumulated as more observations were made. In this situation, the natural question was whether these observations indicated faults in the theory itself or merely shortcomings in our ability to observe the Universe.

With the advent of Albert Einstein's theory of general relativity, this question was partly resolved as it describes the effect of gravity on time and space more accurately than before. General relativity together with the standard model of particle physics, developed throughout the twentieth century, is able to a describe a major part of the peculiarities our Universe exhibits.

Once again deviations from the expected results were observed when the Dutch astronomer Jan Oort studied the orbital velocities of stars in the Milky Way. He concluded that there had to be more matter in the galaxy than could be detected through direct methods. This missing matter was named *dark matter* [2]. Since then, much research has been devoted to dark matter but no candidate for the missing dark matter in the Universe has been detected and confirmed. The presently dominant theory is that the dark matter consists of particles [3]. Still another possibility would be that the laws of gravity and the theory of general relativity are incomplete and merely special cases of yet another, more general, theory.

Although direct evidence for dark matter is scarce, some conclusions can be drawn about its nature from experiments and observations. Dark matter does not seem to interact with "ordinary" matter through either the electromagnetic or strong interaction [4], making it problematic to detect. Even though it cannot be seen directly, the impact of dark matter through gravity can be measured. The mass-energy ratio between ordinary matter and dark matter has been shown to be approximately $1:5$ in experiments [5]. Furthermore, the majority of the energy content of the Universe seems to be an altogether different kind of energy, *dark energy*. However, dark energy seems to not interact directly

with matter and will therefore not be studied in detail. Current experiments show that the distribution of the total mass-energy of the universe is 4.9 % ordinary matter, 26.8 % dark matter and 68.3 % dark energy [5].

The prevailing approach to explain and understand dark matter today is to look for a more fundamental theory to replace the standard model. So far, the behavior of all observed particles and interactions has successfully been explained by the standard model. However, to account for dark matter particles, it is now believed that a more general theory exists that coincides with the standard model in the low-energy limit [6].

Dark matter research can be divided into several parts. Firstly, theory predicts different kinds of particles with certain properties. These are then analyzed and compared to experimental data to narrow the possibilities. Lastly, experiments try to detect different particles while continuously refining constraints. The main objective is to find a particle which fulfills all theoretical requirements as well as being experimentally verifiable. The present study focuses on the part where predicted particles are analyzed and compared to experimental data.

This report will start with an introduction of the basic tools for analyzing the abundance of dark matter in the Universe. The theory of an expanding universe tells us that a long time ago, the Universe was much hotter and denser. A model for dark matter will be created based on the assumption that a given species of dark matter was in equilibrium with its surroundings at some point in time. From this model it will be determined at what time the particles fell out of equilibrium due to decrease in temperature. This concept, called freeze-out, will be explained in section 2.4. Moreover, an estimate of the remaining abundance of the species today will be computed and constraints on particle parameters investigated. Finally, the results and conclusions are discussed and suggestions for further research are made.

Chapter 2

Background Material

This chapter will serve to introduce the reader to the basic concepts of cosmology necessary to properly appreciate the content of this report. Introducing convenient units commonly used in this context simplifies several expressions otherwise cluttered with natural constants. An explanation of the units is given in section 2.1. The expanding universe together with the metric of general relativity constitute the framework for cosmology research and are briefly explained in sections 2.2 and 2.3. As the major subject of this report is dark matter, key concepts of dark matter are presented in section 2.4 together with some exploration of the current theories. Finally, section 2.5 contains a thorough derivation of the Boltzmann equation, which is the main tool used in this study to analyze the dark matter abundance.

2.1 Natural Units

Throughout this report, *natural units*, commonly used in cosmology and particle physics, will be used unless otherwise stated. This means that the natural constants $\hbar$, c and k_{B} are set to 1. Keeping the unit electron volt (eV), every other unit can then be expressed in eV by multiplying with an appropriate combination of $\hbar$, c and k_{B}. As an example, the procedure for converting mass in the SI-unit kg to mass in the natural unit eV is

$$\begin{aligned} 1\,\mathrm{kg} &= 1\,\mathrm{kg} \times c^2 \\ &= 8.988 \times 10^{16}\,\mathrm{kg\,m^2\,s^{-2}} \\ &= 8.988 \times 10^{16}\,\mathrm{J}/1.602 \times 10^{-19}\,\mathrm{J/eV} \\ &= 5.610 \times 10^{35}\,\mathrm{eV}. \end{aligned} \tag{2.1}$$

With this convention, the process of converting from any other unit to eV is univocal. Furthermore, metric prefixes can be used together with eV. In this report GeV will be the most frequently used unit.

2.2 The Expanding Universe

The Universe has expanded ever since the Big Bang. It is important to remember that space itself is expanding and that objects are not simply being hurled outwards into "space". This means that the expansion can be described by the *cosmic scale factor*

$a(t)$ which describes how the distance between points at rest with respect to each other evolves in time due to the expansion of the Universe. Only its relative value is relevant as $a(t)$ is a scale factor, therefore it is commonly set to 1 at the present time [7]. It is also convenient to introduce the Hubble parameter

$$H(t) \equiv \frac{\dot{a}(t)}{a(t)}, \tag{2.2}$$

where the dot denotes derivative with respect to time, a convention which will be used throughout this report. A recent measurement shows that the present value of the Hubble parameter is $H_0 = 67.4\,(\mathrm{km/s})/\mathrm{Mpc}$ [5]. Furthermore, it has been confirmed that the expansion of the Universe is presently accelerating, or in mathematical terms $\ddot{a}(t) > 0$ [8]. Consequently, both $a(t)$ and $\dot{a}(t)$ are time dependent implying that $H(t)$, in general, varies with time.

An implication of the expanding universe is that an ambiguity arises when defining distances. Two different distances will be used to describe different phenomena. Firstly, *physical distance* is proportional to the scale factor and constitutes the distance an experiment would measure. Secondly, *comoving distance* is the distance between two coordinates on an imaginary grid which expands together with space itself. The comoving distance between two objects at rest relative to each other will always be the same, regardless of the expansion, whereas the physical distance will be time dependent.

2.3 Metric

A *metric* defines the distance between points in a given metric space. For example in 2D Cartesian coordinates the distance dl is given by

$$dl^2 = dx^2 + dy^2.$$

For small distances, the same distance expressed in polar coordinates is

$$dl^2 = dr^2 + r^2 d\theta^2,$$

where x and y are the Cartesian coordinates and r and θ are the polar coordinates. Even though the distances are calculated differently, the result is invariant with respect to coordinate system. Thus, the metric acts on coordinates to produce a coordinate-invariant measure of distance. Another way to express this is by using tensors,

$$dl^2 = g_{ij} x^i x^j,$$

where g_{ij} is the metric tensor. Throughout this report we use the Einstein summation convention, which means that terms are summed over repeated indices. Roman indices are summed over the three spatial coordinates, while Greek indices are summed over the four spacetime coordinates.

The commonly used metric associated with an expanding universe is

$$g_{\mu\nu} = \begin{pmatrix} -1 & 0 & 0 & 0 \\ 0 & a^2(t) & 0 & 0 \\ 0 & 0 & a^2(t) & 0 \\ 0 & 0 & 0 & a^2(t) \end{pmatrix}, \tag{2.3}$$

where the first element is temporal and the remaining are spatial. This is the metric that will be used throughout this report. By assuming that the Universe is homogeneous and isotropic on large scales, the scale factor $a(t)$ becomes space invariant. These assumptions simplify the mathematics and are supported by experiments [9]. Furthermore, we will need the Christoffel symbol

$$\Gamma^{\mu}_{\alpha\beta} \equiv \frac{g^{\mu\nu}}{2}\left(\frac{\partial g_{\alpha\nu}}{\partial x^{\beta}} + \frac{\partial g_{\beta\nu}}{\partial x^{\alpha}} - \frac{\partial g_{\alpha\beta}}{\partial x^{\nu}}\right), \tag{2.4}$$

which contains information of the curvature of space. It will be used in section 2.5 to describe an expanding universe. A rigorous derivation is beyond the scope this report.

2.4 Introduction to Dark Matter

2.4.1 Dark Matter Abundance

Most of the common theories describing dark matter assumes that the dark matter we observe constitutes of different kinds of particles, called *species*. The particles emit no electromagnetic radiation and are therefore only detectable through their gravitational interaction with ordinary matter.

In the early Universe, interactions were frequent as a consequence of the energetic environment. Due to the high interaction rate, it is possible to assume that every allowed interaction occurs at a frequency high enough to ensure that any deviations from equilibrium quickly diminishes. Thus, the dark matter particles are believed to have been in *thermodynamical equilibrium*. This means that they were in mechanical, chemical, thermal and radiative equilibrium. As the Universe expanded, the interaction rate between dark matter and ordinary matter decreased, causing the particles to *decouple*. Essentially, decoupling means that the particles stop interacting and the number of particles after decoupling, the *relic abundance*, will remain roughly constant. Decoupling is a continuous process, as will be shown in chapter 3, but it is quick compared to the age of the Universe due to the expansion of space as well as decrease in temperature [10]. Before decoupling, the distribution of dark matter is simply given by the Boltzmann distribution as it is in thermodynamical equilibrium. The evolution of dark matter out of equilibrium is harder to predict and is given by the *Boltzmann equation* presented in section 2.5. This process, where the species starts in equilibrium and eventually decouples, is called the *freeze-out scenario* and decoupling itself is sometimes referred to as *freeze-out*.

The concept of *critical density* ρ_{c} is commonly used in cosmology. In a simplified model with no dark energy one can think of the critical density as the mass-energy density if the Universe contains exactly enough mass to be the watershed point between expanding forever and collapsing. This special case is called a *flat universe*. If the density is any higher, the expansion of the Universe will slow down and eventually start to contract, a *closed universe*. On the other hand, if the density is lower, the Universe would keep expanding forever, an *open universe*. It is possible to derive the expression

$$\rho_{\mathrm{c}} = \frac{3H^2}{8\pi G} \tag{2.5}$$

directly from the Friedmann equations in a model without dark energy [11]. Including dark energy is complicated because it is different from all other kinds of matter and

energy in the sense that dark energy is expanding space itself which drags everything along with it.

Quantification of a substance can be made through the *density parameter* defined as

$$\Omega \equiv \frac{\rho}{\rho_c} = \frac{8\pi G\rho}{3H^2}, \tag{2.6}$$

which basically is the ratio between the density ρ of the relevant substance and the critical density. The matter, dark matter and dark energy quantities will henceforth be given the subscripts M, DM and Λ respectively. According to recent measurements, the total density is equal to the critical density and the distribution is as follows: $\Omega_{\mathrm{M}} = 4.9\,\%$, $\Omega_{\mathrm{DM}} = 26.8\,\%$ and $\Omega_\Lambda = 68.3\,\%$ [5].

2.4.2 Evidence

An indication of the existence of dark matter was given by analysis of the rotational velocity of galaxies, as mentioned in chapter 1. Using Kepler's third law it can be expected that the rotational velocity as a function of distance from the center will follow

$$v(r) = \sqrt{\frac{GM(r)}{r}}, \tag{2.7}$$

where r is the distance from the center, G is Newton's gravitational constant and $M(r)$ is the total mass within the radius r. The mass $M(r)$ is given by

$$M(r) = 4\pi \int_0^r \rho(r) r^2 \,\mathrm{d}r, \tag{2.8}$$

where $\rho(r)$ is the mass density, under the assumption of spherical symmetry. We would expect that $v(r) \propto 1/\sqrt{r}$ for large r where a low density is observed. In practice, measurements are made on hydrogen clouds orbiting outside the luminous parts of the galaxy. However, measurements show that v is in fact almost constant in the region where a decrease would be expected [12]. Thus, $M \propto r$ and consequently $\rho \propto 1/r^2$ [13].

There are several other pieces of evidence supporting the existence of dark matter such as:

- Strong gravitational lensing by elliptical galaxies [14].
- Mass-to-light ration inferred from velocity dispersion of galaxies in clusters [15].
- Analysis of cosmic microwave background anisotropies [16].

2.4.3 Candidates

There are several dark matter candidates since very little is known about their nature and few constraints can be made. The parameter values for different candidates often span several orders of magnitude. For example, the masses of proposed dark matter particles span more than 20 orders of magnitude [10]. In the freeze-out scenario studied in this report, a common candidate is a *weakly interacting massive particle*, often referred to as WIMP. As indicated by their name, WIMPs are relatively heavy and are presumed to only

interact through gravitation and the weak force [10]. Relatively heavy in this context means that the particle mass is roughly in the order of 10^{11} eV. One of the reasons why WIMPs are popular is because the parameter values predicted by theory yields the correct relic abundance, a phenomenon sometimes called "the WIMP miracle" [17]. Besides WIMPs, there exists a plethora of different candidates. A comprehensive review of several candidates can be found in the work of Bertone et al. [10].

2.5 The Boltzmann Equation

2.5.1 The Liouville Operator

The evolution of the phase space distribution of particles $f(\boldsymbol{p}, \boldsymbol{x}, t)$ is governed by the Boltzmann equation

$$\mathbf{L}[f] = \mathbf{C}[f], \tag{2.9}$$

where

$$\mathbf{L} = p^\alpha \frac{\partial}{\partial x^\alpha} - \Gamma^\alpha_{\beta\gamma} p^\beta p^\gamma \frac{\partial}{\partial p^\alpha} \tag{2.10}$$

is the Liouville operator and $\mathbf{C}$ is the collision operator [18]. The collision operator describes interactions between particles and will be introduced in section 2.5.2. Firstly, we can observe that only derivatives of f appear on the left-hand side of eq. (2.9). The two derivatives are with respect to $\boldsymbol{x}$ and $\boldsymbol{p}$ respectively, implying that the change in the phase space distribution with respect to space and momentum depends on the interactions of particles.

We assume that the phase space distribution function is both homogeneous and isotropic, so that $f(\boldsymbol{p}, \boldsymbol{x}, t) = f(E, t)$. Under these assumptions the Liouville operator (2.10) acting on f takes on a simpler form. Recalling that $p^0 = E$, the first term collapses to just the temporal term of the implicit sum. For the same reason, the second term disappears for all values of the summation index α, except when $\alpha = 0$. Since $\Gamma^0_{00} = \Gamma^0_{i0} = \Gamma^0_{0i} = 0$ and $\Gamma^0_{ij} = \delta_{ij} \dot{a} a$ we obtain

$$\mathbf{L}[f] = E \frac{\partial f}{\partial t} - H p^2 \frac{\partial f}{\partial E}, \tag{2.11}$$

where we have used the fact that $p^i p^i = g^{ij} p_j p^i = a^{-2} p^2$ (where, in the last expression, p is the norm of the spatial momentum vector and the 2 is an exponent, not a contravariant index) and used definition (2.2) of the Hubble parameter.

Consider the Boltzmann equation (2.9). Using the expression in eq. (2.11), multiplying both sides by $\mathrm{d}^3 p / ((2\pi)^2 E)$ and integrating over the whole phase space we obtain

$$\int \frac{\partial f}{\partial t} \frac{\mathrm{d}^3 p}{(2\pi)^3} - H \int \frac{p^2}{E} \frac{\partial f}{\partial E} \frac{\mathrm{d}^3 p}{(2\pi)^3} = \int \frac{\mathbf{C}[f]}{E} \frac{\mathrm{d}^3 p}{(2\pi)^3}. \tag{2.12}$$

In the first term the derivative with respect to t can be moved outside the integral. For the second term we note that, since $E = \sqrt{p^2 + m^2}$,

$$\frac{\partial E}{\partial p} = \frac{1}{2} \frac{1}{\sqrt{p^2 + m^2}} 2p = \frac{p}{E}, \tag{2.13}$$

and we can use $\dfrac{\partial f}{\partial p} = \dfrac{\partial f}{\partial E}\dfrac{\partial E}{\partial p}$ to rewrite the second term as

$$H \int \frac{p^2}{E}\frac{\partial f}{\partial E}\frac{\mathrm{d}^3 p}{(2\pi)^3} = \frac{H}{(2\pi)^3}\int p\frac{\partial f}{\partial p}\,\mathrm{d}^3 p. \tag{2.14}$$

Invoking our assumption of homogeneity and isotropy we can integrate the angular parts of the integral, which introduces an overall factor 4π and a factor p^2 in the integrand. This leaves a one-dimensional integral of p from 0 to ∞. A simple calculation shows that, demanding the integral of f over all phase space to be finite, f must fall to zero faster than p^{-3} as $p \to \infty$. Thus, using integration by parts on the right-hand side integral of eq. (2.14) we obtain

$$\frac{4\pi H}{(2\pi)^3}\int_0^\infty p^3\frac{\partial f}{\partial p}\,\mathrm{d}p = \frac{4\pi H}{(2\pi)^3}\left(\left[p^3 f\right]_0^\infty - 3\int_0^\infty p^2 f\,\mathrm{d}p\right), \tag{2.15}$$

where the bracketed term disappears. We can revert this to an integral over the whole phase space again by eliminating the factors 4π and p^2 from the integrand.

By expressing the number density $n(t)$ as

$$n(t) = \frac{g}{(2\pi)^3}\int f(E,t)\,\mathrm{d}^3 p, \tag{2.16}$$

where g is the degeneracy, we can finally rewrite the left-hand side of eq. (2.12). Using eqs. (2.13) through (2.16), as well as incorporating g into f, we can rewrite eq. (2.12) as

$$\frac{\mathrm{d}n}{\mathrm{d}t} + 3Hn = \int \frac{\mathbf{C}[f]}{E}\frac{\mathrm{d}^3 p}{(2\pi)^3}. \tag{2.17}$$

2.5.2 The Collision Operator

We now turn our attention to the right-hand side of eq. (2.17), the expression containing information about the interactions of different species. Consider a process

$$\psi + a + b + \cdots \leftrightarrow i + j + \cdots,$$

where ψ is the dark matter species of interest. Then, the right-hand side of eq. (2.17) is given by

$$\begin{aligned}\int \frac{\mathbf{C}[f]}{E}\frac{\mathrm{d}^3 p}{(2\pi)^3} = &-\frac{1}{g}\int \mathrm{d}\Pi_\psi \mathrm{d}\Pi_a \mathrm{d}\Pi_b \cdots \mathrm{d}\Pi_i \mathrm{d}\Pi_j \\ &\times (2\pi)^4\delta^4(p_\psi + p_a + p_b + \cdots - p_i - p_j - \cdots) \\ &\times \Big[|\mathcal{M}|^2_{\psi+a+b+\cdots\to i+j+\cdots} f_a f_b \cdots f_\psi (1 \pm f_i)(1 \pm f_j)\cdots \\ &- |\mathcal{M}|^2_{i+j+\cdots\to\psi+a+b+\cdots} f_i f_j \cdots (1 \pm f_a)(1 \pm f_b)\cdots(1 \pm f_\psi)\Big],\end{aligned} \tag{2.18}$$

where δ^4 is the four-dimensional Dirac delta function, p_z and f_z are the four-momentum and phase space distribution for species z respectively and $\mathcal{M}$ denotes the amplitude of the process and corresponds to the strength of the interaction [13]. Starting from the top, with the definition

$$\mathrm{d}\Pi_z \equiv \frac{g_z}{(2\pi)^3}\frac{\mathrm{d}^3 p_z}{2E_z}, \tag{2.19}$$

the first line of eq. (2.18) tells us that we must sum over the whole phase space for every particle to obtain all interactions. Secondly, the next line enforces the conservation of momentum and energy upon the process. Lastly, the two remaining lines represent the rate of the process going one way or the other. Thus, the production of ψ (together with $a, b, \cdots$) is proportional to $f_i f_j \cdots$ and the opposite process is proportional to $f_\psi f_a f_b \cdots$.

Simplifications of eq. (2.18) can be made. By assuming that the interaction is reversible, we define

$$|\mathcal{M}| \equiv |\mathcal{M}|_{\psi+a+b+\cdots \to i+j+\cdots} = |\mathcal{M}|_{i+j+\cdots \to \psi+a+b+\cdots}$$

Our next assumption is the absence of degenerate matter and Bose-Einstein condensates. This allows us to use Maxwell-Boltzmann statistics as well as approximate the blocking and stimulated emission factor $1 \pm f_x \approx 1$ for all species. To summarize, we have

$$\begin{aligned}\frac{\mathrm{d}n_\psi}{\mathrm{d}t} + 3Hn_\psi = &- \int \mathrm{d}\Pi_\psi \mathrm{d}\Pi_a \mathrm{d}\Pi_b \cdots \mathrm{d}\Pi_i \mathrm{d}\Pi_j (2\pi)^4 |\mathcal{M}|^2 \\ &\times \delta^4(p_\psi + p_a + p_b + \cdots - p_i - p_j - \cdots)[f_a f_b \cdots f_\psi - f_i f_j \cdots]. \end{aligned} \tag{2.20}$$

Investigating eq. (2.20) we observe that the change in the number density over time can be described by two terms. One term accounts for all interactions by which the species in question is created or annihilated and one term is a direct consequence of the expansion of the Universe, $3Hn_\psi$.

2.5.3 A Change of Variables

As the effect of the species being diluted by the expansion of the Universe is trivial, the number of particles per comoving volume will be introduced. Using the fact that entropy per comoving volume is conserved, the new variable

$$Y \equiv \frac{n_\psi}{s} \tag{2.21}$$

is defined. The entropy density s is given by

$$s = \frac{2\pi^2}{45} g_{*S} T^3, \tag{2.22}$$

where g_{*S} is the number of relativistic degrees of freedom for entropy [13]. Conservation of the entropy density in comoving volume is expressed as

$$\frac{\mathrm{d}(sa^3)}{\mathrm{d}t} = 0. \tag{2.23}$$

Taking the derivative of Y with respect to time we thus end up with

$$\frac{\mathrm{d}Y}{\mathrm{d}t} = s^{-1}\left(\frac{\mathrm{d}n_\psi}{\mathrm{d}t} + 3Hn_\psi\right), \tag{2.24}$$

where definition (2.2) of the Hubble parameter has been used. Apart from the overall factor s^{-1}, eq. (2.24) is identical to the left-hand side of eq. (2.20).

In cosmology, it can be useful to measure temporal evolution in a suitable strictly monotonic function of t, other than time itself, when time is not the quantity which is

of physical relevance. When studying the evolution of the Universe, the natural measure of time is usually the temperature T which is a strictly decreasing function of t. In the early Universe the relationship between t and T is given by

$$t = 0.301 \times g_*^{-\frac{1}{2}} \frac{m_{\mathrm{Pl}}}{T^2}, \tag{2.25}$$

where m_{Pl} is the Planck mass and g_* is the effective number of relativistic degrees of freedom [13].

In the problem at hand it is convenient to define

$$x \equiv \frac{m}{T}, \tag{2.26}$$

where m is the mass of the particle, as a measure of time. Using the chain rule, eqs. (2.24) and (2.25) as well as definition (2.26) of x, we have

$$\frac{\mathrm{d}Y}{\mathrm{d}x} = \frac{\mathrm{d}Y}{\mathrm{d}t}\frac{\mathrm{d}t}{\mathrm{d}x} = s^{-1}\left(\frac{\mathrm{d}n_\psi}{\mathrm{d}t} + 3Hn_\psi\right)\left(0.602 \times g_*^{-\frac{1}{2}} \frac{m_{\mathrm{Pl}}}{m^2} x\right). \tag{2.27}$$

The rightmost parenthesized factor is a formulation of the Hubble parameter at time $x = 1$ [13]. By defining

$$H(m) \equiv 1.66 \times g_*^{1/2} m^2 / m_{\mathrm{Pl}} = H(x)x^2, \tag{2.28}$$

we can use eq. (2.20) together with eq. (2.27) to restate the Boltzmann equation in terms of Y and x,

$$\begin{aligned}\frac{\mathrm{d}Y}{\mathrm{d}x} = &-\frac{x}{H(m)s}\int \mathrm{d}\Pi_\psi \mathrm{d}\Pi_a \mathrm{d}\Pi_b \cdots \mathrm{d}\Pi_i \mathrm{d}\Pi_j (2\pi)^4 |\mathcal{M}|^2 \\ &\times \delta^4(p_\psi + p_a + p_b + \cdots - p_i - p_j - \cdots)[f_a f_b \cdots f_\psi - f_i f_j \cdots].\end{aligned} \tag{2.29}$$

The general Boltzmann equation (2.9) has now been simplified using the following assumptions:

- The Universe is homogeneous and isotropic.
- Maxwell-Boltzmann statistics are valid.
- The processes are reversible.

All of the assumptions above are general, thus eq. (2.29) holds for any particle in the Universe. Exploiting specific properties of the dark matter in our model, it will be further developed in section 3.2.

Chapter 3

Investigation

3.1 Problem

One of the key questions in dark matter research is how much dark matter would remain today, under certain assumptions about the initial state of the Universe and properties of the dark matter particles. In this report, the freeze-out scenario will be the primary approach to analyze the dark matter evolution. Supposing that the abundance at an earlier time is known, it is possible to calculate the relic density today using the Boltzmann equation developed in section 2.5. On the other hand, using experimental values of the present dark matter density of the Universe, the Boltzmann equation can be used to put specific constraints on the dark matter particle parameters. We will argue that the relevant free parameters are the thermally averaged cross section, introduced in section 3.2, and the particle mass. Having to consider only these two parameters will allow us to put stringent constraints on the parameter space.

In section 3.2.1 the Boltzmann equation from section 2.5 will be further modified to analyze relic abundances in the freeze-out model. Section 3.2.2 discusses the relation between Y and the density parameter Ω. The differential equation for the relic abundance is analyzed and approximate analytical expressions for the present relic abundance are derived in section 3.3. The numerical analysis of the Boltzmann equation is described in section 3.4. The results are presented in section 3.5 and discussed in section 3.6.

3.2 Model

3.2.1 The Boltzmann Equation for Dark Matter

The dark matter species are assumed to be stable and only interact through an annihilation process

$$\psi\bar{\psi} \longleftrightarrow X\bar{X}.$$

As in section 2.5, ψ will be used to denote the dark matter particle and $\bar{\psi}$ its antiparticle. Furthermore, an equal number of ψ and $\bar{\psi}$ is assumed. Daughter particles and antiparticles are denoted generically by X and $\bar{X}$ respectively. Energy conservation of the interactions ensures that

$$E_\psi + E_{\bar{\psi}} = E_X + E_{\bar{X}}. \tag{3.1}$$

Assuming that the daughter particles remain in equilibrium, their distribution functions are $f_X = \exp\left(-E_X/T\right)$ and $f_{\bar{X}} = \exp\left(-E_{\bar{X}}/T\right)$.

Proceed by manipulating the product

$$f_X f_{\bar{X}} = e^{-\frac{E_X+E_{\bar{X}}}{T}} = e^{-\frac{E_\psi+E_{\bar{\psi}}}{T}} = f_\psi^{\mathrm{EQ}} f_{\bar{\psi}}^{\mathrm{EQ}} \tag{3.2}$$

using energy conservation from eq. (3.1). Henceforth, EQ will denote equilibrium. The reformulation

$$\begin{aligned}\frac{\mathrm{d}Y}{\mathrm{d}x} = &-\frac{x}{H(m)s}(2\pi)^4 \int \mathrm{d}\Pi_\psi \int \mathrm{d}\Pi_{\bar{\psi}} \int \mathrm{d}\Pi_X \int \mathrm{d}\Pi_{\bar{X}} |\mathcal{M}|^2 \\ &\times \delta^4\left(p_\psi + p_{\bar{\psi}} - p_X - p_{\bar{X}}\right)\left[f_\psi f_{\bar{\psi}} - f_\psi^{\mathrm{EQ}} f_{\bar{\psi}}^{\mathrm{EQ}}\right]\end{aligned} \tag{3.3}$$

of eq. (2.29) is now possible. When evaluating the integrals

$$\int f \,\mathrm{d}\Pi = \frac{g}{(2\pi)^3}\int e^{-E/T}\,\frac{\mathrm{d}^3p}{2E}, \tag{3.4}$$

it is possible to use eq. (2.16), leaving

$$\frac{g}{(2\pi)^3}\int e^{-E/T}\,\frac{\mathrm{d}^3p}{2E} = n\, n_{\mathrm{EQ}}^{-1}\int f_{\mathrm{EQ}}\,\mathrm{d}\Pi. \tag{3.5}$$

Rewriting the integrals in eq. (3.3) yields

$$\frac{\mathrm{d}Y}{\mathrm{d}x} = -\frac{x}{H(m)s}\langle\sigma v\rangle\left[n_\psi n_{\bar{\psi}} - n_\psi^{\mathrm{EQ}} n_{\bar{\psi}}^{\mathrm{EQ}}\right], \tag{3.6}$$

where the definition of the *thermally averaged annihilation cross section*

$$\begin{aligned}\langle\sigma v\rangle \equiv &(2\pi)^4\left(n_\psi^{\mathrm{EQ}}\right)^{-2}\int \mathrm{d}\Pi_\psi \int \mathrm{d}\Pi_{\bar{\psi}} \int \mathrm{d}\Pi_X \int \mathrm{d}\Pi_{\bar{X}}\,|\mathcal{M}|^2 \\ &\times \delta^4\left(p_\psi + p_{\bar{\psi}} - p_X - p_{\bar{X}}\right)\, e^{-E_\psi/T} e^{-E_{\bar{\psi}}/T}\end{aligned} \tag{3.7}$$

is used. The cross section essentially contains information of how likely collisions between particles are, similarly to a classical cross section. Furthermore, using the change of variables introduced in definition (2.21), with Y_{EQ} defined analogously, and where $H(m)$ is expressed using definition (2.28), eq. (3.6) can be expressed as

$$\frac{\mathrm{d}Y(x)}{\mathrm{d}x} = -\frac{x\langle\sigma v\rangle s}{H(m)}\left[Y(x)^2 - Y_{\mathrm{EQ}}(x)^2\right]. \tag{3.8}$$

Finally, using eqs. (2.22) and (2.28), we find that by defining

$$\lambda \equiv \left[\frac{x\langle\sigma v\rangle s}{H(m)}\right]_{x=1} = 0.264 \times m_{\mathrm{Pl}} m \sigma_0 \frac{g_{*S}}{\sqrt{g_*}}, \tag{3.9}$$

where σ_0 is $\langle\sigma v\rangle$ at time $x = 1$, the reformulation

$$\frac{\mathrm{d}Y(x)}{\mathrm{d}x} = -\frac{\lambda}{x^2}\left[Y(x)^2 - Y_{\mathrm{EQ}}(x)^2\right] \tag{3.10}$$

can be made. It has now implicitly been assumed that $\langle\sigma v\rangle$ is independent of x, thus $\sigma_0 = \langle\sigma v\rangle$ in the model used. The function λ is chosen to be independent of x by letting $x = 1$ and leaving the dependence of x in the factor x^{-2}. Thus, λ can be treated as a constant within certain limits. A detailed discussion of λ is found in section 3.6.1.

3.2.2 Quantification of Relic Abundance

Up to this point, quantification of the abundance has been expressed by Y. This is convenient for the mathematical analysis but when comparing calculated values to measured ones, the density parameter Ω will be used. The relation between Y and Ω is given by

$$\Omega_0 = \frac{ms_0Y_0}{\rho_c} = \frac{8\pi G m s_0 Y_0}{3H^2}, \tag{3.11}$$

where the second equality is given by eq. (2.5). The subscript 0 denotes the present day value and $s_0 = 2889.2\,\mathrm{cm}^{-3}$ is the entropy density assuming three Dirac neutrino species [10]. By inserting numerical values and converting to natural units, the relation

$$\Omega_0 = 6.04 \times 10^8 \frac{m}{\mathrm{GeV}} Y_0 \tag{3.12}$$

is obtained.

3.3 Analytical Calculations

The relic density of a particular dark matter species is determined by eq. (3.10) which is a Riccati differential equation. It is ordinary and non-linear and no closed-form analytical solutions are known. However, we can use the physics behind the equation to extract some information from it.

3.3.1 Freeze-out Scenario

In the early universe, when x is small, the dark matter species is expected to have been in thermal equilibrium with its surroundings. In thermal equilibrium, the initial condition is $Y = Y_{\mathrm{EQ}}$. Consequently, by analyzing eq. (3.10), we conclude that $\mathrm{d}Y/\mathrm{d}x = 0$.

The function Y will initially follow Y_{EQ}, but eventually the x^{-2} factor will dominate the $(Y^2 - Y_{\mathrm{EQ}}^2)$ factor and Y will remain roughly constant while Y_{EQ} continues to decrease. The point at which Y stops tracing Y_{EQ} is the freeze-out and the values of Y and x at freeze-out are denoted by Y_{f} and x_{f}, respectively.

Consider a *hot relic*, which decouples while relativistic. This will be the case if $x_{\mathrm{f}} \lesssim 3$. For $x \lesssim 3$, Y_{EQ} stays approximately constant, so the asymptotic value of Y as $x \to \infty$, Y_∞, will be

$$Y_\infty \approx Y_{\mathrm{EQ}}(x_{\mathrm{f}}). \tag{3.13}$$

In this case it is hard to precisely define the freeze-out time x_{f}. However, since Y will stay approximately constant, a precise definition of x_{f} is not necessary to make an order of magnitude approximation of Y_∞.

A *cold relic* decouples when non-relativistic, that is $x_{\mathrm{f}} \gtrsim 3$. At early times Y will trace Y_{EQ}. As the temperature drops and the species decouple, annihilations do not occur frequently enough to maintain equilibrium anymore. Subsequently Y_{EQ} will become much smaller than Y and the right-hand side of eq. (3.10) will be dominated by the Y^2 term for $x > x_{\mathrm{f}}$. This allows us to simplify the equation to

$$\frac{\mathrm{d}Y}{\mathrm{d}x} \approx -\frac{\lambda}{x^2} Y^2 \tag{3.14}$$

which is an analytically solvable separable ordinary differential equation. Upon integration from x_f to ∞, eq. (3.14) yields

$$\frac{1}{Y_\infty} - \frac{1}{Y_\mathrm{f}} = \frac{\lambda}{x_\mathrm{f}}. \tag{3.15}$$

At sufficiently late times, Y will be smaller than at freeze-out. Thus, a rough approximation of the relic density after freeze-out can be made,

$$Y_\infty \approx \frac{x_\mathrm{f}}{\lambda}. \tag{3.16}$$

3.3.2 Determining the Freeze-out Time

Although we derived an approximate expression in eq. (3.16) for determining the present relic density, it still depends on the freeze-out time, which has so far only been vaguely defined. For a cold relic, where the deviation from equilibrium is immediately apparent, an expression for the freeze-out time can be derived. We introduce a well-chosen constant c of order unity such that

$$Y_\mathrm{f} = (c+1)Y_\mathrm{EQ}(x_\mathrm{f}). \tag{3.17}$$

Substituting eq. (3.17) into (3.15) yields an equation with only x_f unknown. It is, however, problematic to solve analytically. A numerical approximation of the solution is

$$x_\mathrm{f} \approx \ln\left[(2+c)\lambda ac\right] - \frac{1}{2}\ln\ln\left[(2+c)\lambda ac\right], \tag{3.18}$$

where $a = 0.145\left(g/g_{*S}\right)$ [13].

3.3.3 Relation between $\langle\sigma v\rangle$ and m

Combining eqs. (3.16) and (3.18), it is possible to show that

$$mY_\infty \approx \frac{m}{\lambda}\left(\ln[(2+c)\lambda ac] - 1/2\ln\ln[(2+c)\lambda ac]\right). \tag{3.19}$$

When making an order of magnitude estimate, the $\ln\ln$-term can be neglected, in this context, as it will typically be at least an order of magnitude smaller than the ln-term. Using definition (3.9),

$$mY_\infty \approx \frac{m\ln\left((2+c)c \times 0.145 \times 0.264 \times m_\mathrm{Pl} m\langle\sigma v\rangle g/\sqrt{g_*}\right)}{0.264 \times m_\mathrm{Pl} m\langle\sigma v\rangle g_{*S}/\sqrt{g_*}} \tag{3.20}$$

is obtained. This can be reformulated, by collecting constants in K, as

$$\langle\sigma v\rangle mY_\infty \propto \ln\left(Km\langle\sigma v\rangle\right), \tag{3.21}$$

when only studying the relation between $\langle\sigma v\rangle$ and m. Finally, experiments constrains the factor mY_∞ allowing us to treat it as a constant implying that it can be neglected leading to

$$\langle\sigma v\rangle \propto \ln(m) + \ln\left(\langle\sigma v\rangle\right). \tag{3.22}$$

3.4 Numerical Analysis

Numerical methods are used to calculate $Y(x)$ using eq. (3.10) for different cases. For practically all cases studied, λ will at least be in the order of 10^8. This results in a numerically stiff equation which essentially means that it is difficult to integrate using numerical methods. It is possible to circumvent this by introducing the change of variables

$$W(x) \equiv \ln(Y(x)), \tag{3.23}$$

with W_{EQ} defined analogously, as made by Steigman et al. [19], leading to the reformulation

$$\frac{\mathrm{d}W}{\mathrm{d}x} = \frac{\lambda}{x^2}\left[e^{2W_{\text{EQ}}-W} - W\right] \tag{3.24}$$

of eq. (3.10). Firstly, W varies over fewer orders of magnitude which greatly decreases the computational power required to solve the equation. Secondly, it is now possible to obtain fairly accurate solutions even when using low precision which was practically impossible in the original, stiffer form.

The general approach taken is to solve eq. (3.24) in the interval $10^0 \leq x \leq 10^3$ and then transform $W(x)$ back to $Y(x)$ using definition (3.23). Furthermore, the relic density today Ω_0 is given by eq. (3.12) where $Y(10^3) = Y_\infty$ is assumed. By varying the parameters and calculating the corresponding relic density, it is possible to set up constraints on the parameter space. One of the main purposes of the numerical analysis is to find the $\langle\sigma v\rangle$ necessary to obtain the correct abundance today for different m. Moreover, numerical solutions can be used to verify the analytical approximation (3.16).

3.5 Results

A family of solutions to eq. (3.10) is shown in fig. 3.1. The figure illustrates the concept of freeze-out as well as the implications of an increasing cross section. For $x < 10$, the solution closely tracks equilibrium due to the high interaction rate. Freeze-out is where Y starts to deviate from equilibrium which is at $x \approx 25$ for the specific parameter values used. At this point, the expansion rate of the universe starts to overshadow the interaction rate in the sense that particles have drifted apart to such an extent that interactions are not frequent enough to maintain equilibrium. Consequently, it is possible to observe how the solution decreases more slowly and becomes almost constant, it freezes-out. The implication of an increasing cross section is that it allows the particles to remain in equilibrium for a longer period since they interact more easily. Subsequently, if the particles remain in equilibrium until a later time, the relic abundance will decrease since the equilibrium abundance drops exponentially.

Figure 3.2 shows the numerically calculated relation between $\langle\sigma v\rangle$ and m in a model where they are the only parameters. With only two parameters it is possible to use the relic abundance, obtained through experiments, as a constraint allowing us to correlate $\langle\sigma v\rangle$ to m. Since the semi-log plot basically is a straight line, there is reason to believe that

$$\langle\sigma v\rangle \propto \log(m) \tag{3.25}$$

within the interval $10^1\,\text{GeV} \leq m \leq 10^4\,\text{GeV}$ with the model used. In fig. 3.2, it is possible to observe that $\langle\sigma v\rangle$ varies roughly a factor 1.4 while m which varies over 3 orders of magnitude. Hence, the relic abundance is more sensitive to differences in $\langle\sigma v\rangle$ than m.

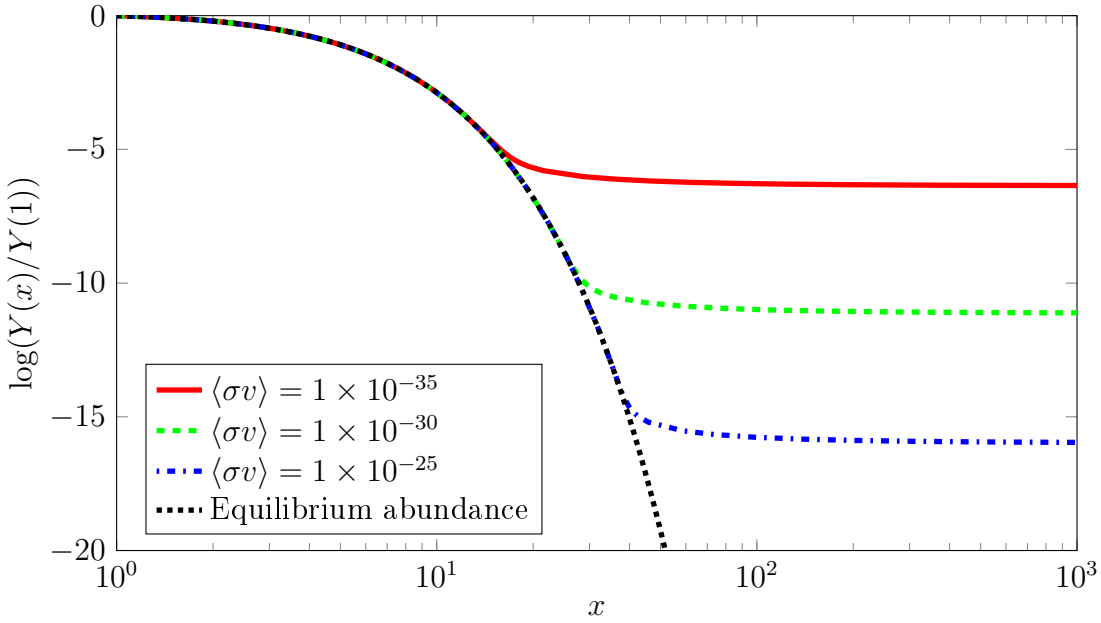

Figure 3.1: Solutions to eq. (3.10) for different values of the parameter $\langle\sigma v\rangle$ in a model where all other parameters are fixed. The concept of remaining in equilibrium, freeze-out and being decoupled are shown.

Two of the introduced methods of calculating Y_∞ are using the analytical approximation (3.16) and numerically solving eq. (3.10). It is reasonable to consider the numerical solution $Y_{\infty,\mathrm{N}}$ to be exact when compared to the analytical approximation $Y_{\infty,\mathrm{A}}$. Consequently, it is possible to investigate the error in the analytical approximation for different values of λ. The agreement between the two methods is shown in fig. 3.3 where the well-chosen constant c has been set to 0.6 and the top x-axis is calculated using approximation (3.18). Considering the error caused by all simplifications made, the ratio $Y_{\infty,\mathrm{N}}/Y_{\infty,\mathrm{A}}$ can be considered to be close to 1 within the studied interval of λ.

3.6 Discussion

3.6.1 Remarks on λ

Throughout the analysis, definition (3.9) of λ has been used. It relies on eq. (2.25) and definition (2.28) which are both limited but spans the relevant time interval. It has been assumed that $g_* = g_{*S} = 100$ which is a good approximation for $T > 0.1\,\mathrm{GeV}$ [13]. This is what determines the limit for large x_f. Despite the limitations on the temperature, the model has been used to describe evolution until $x = m/T = 10/T = 10^3$ implying that $T = 0.01\,\mathrm{GeV}$. This is acceptable as the time of freeze-out is roughly $x = 10$ which is within the range of the model. Hence, any errors caused by inaccuracies in the model are negligible since the abundance after freeze-out is nearly constant almost regardless of the model and parameters. Moreover, it has been assumed that only s-wave annihilation is allowed. The details of the annihilation process itself is beyond the scope of this report but essentially the assumption implies that $\langle\sigma v\rangle$ is independent of x and that the power

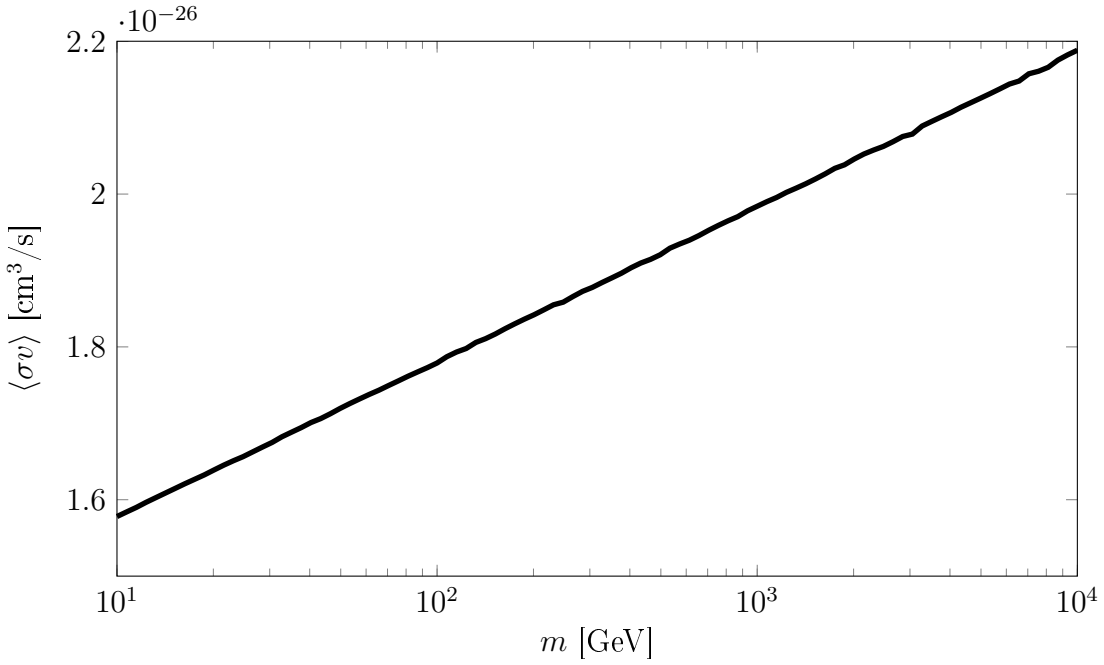

Figure 3.2: The relation between $\langle \sigma v \rangle$ and m in a model where they are the only two parameters and experimental data is used as a constraint.

of x in the denominator in eq. (3.10) is 2. It is then reasonable to assume that the model used is limited to a certain interval but still able to fulfill its purpose within acceptable tolerances.

Limitations at early times in the freeze-out model is determined by the validity of eq. (2.25) and definition (2.28) upon which λ relies. They are important to remember since other scenarios might include times which requires other models to describe the relation between T and t or the expansion of the Universe. It is x_f that determines the necessary model since the evolution before x_f is described by equilibrium and is simply constant after x_f.

One notable characteristic of the solutions to eq. (3.10) is that larger λ yields lower relic densities, which is an expected result. This phenomenon can be seen in fig. 3.1. Firstly, this is in accordance with the analytical result (3.16). Secondly, the physical explanation is that the probability of particles interacting is proportional to λ. Consequently, as remaining in equilibrium requires a high interaction rate, the time of freeze-out also increases for increasing λ. As a result, the relic density will decrease due to a later freeze-out. Furthermore, large λ also motivates the assumption that the dark matter particles were initially in equilibrium. This will be further discussed in section 3.6.3.

The opposite scenario, when λ is small, is more complicated because assumption that the dark matter particles remained in thermal equilibrium at early times might not be applicable. This is divided into two different cases, either the particles were created at some time and never reached equilibrium, the *freeze-in scenario*, or the particles have been in equilibrium at a time where the model described in section 3.2 is inapplicable.

Freeze-in is essentially described by the same mathematical framework even though the physics behind it is slightly different. Particles which freeze-in are assumed to have a negligible initial abundance which at some point in time starts to grow. The freeze-

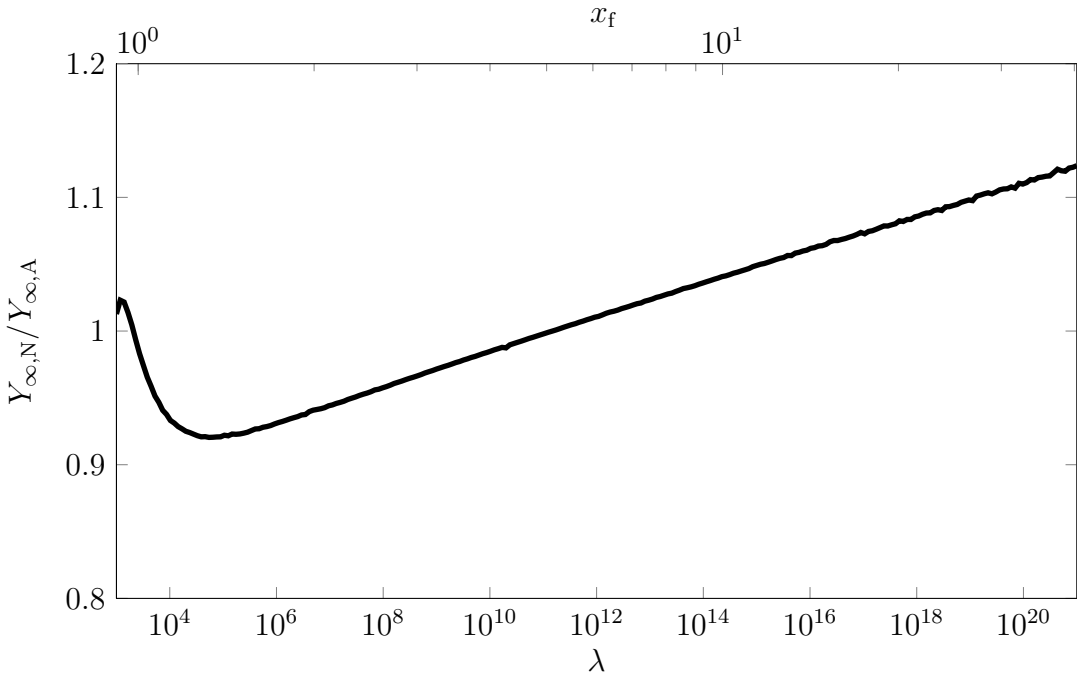

Figure 3.3: Agreement between Y_∞ calculated using the analytical approximation (3.16) with $c = 0.6$ and obtained through numerical solution to eq. (3.10). Top scale shows x_f determined by λ using eq (3.18). The ratio being relatively close to 1 indicates good agreement between analytical and numerical results.

in scenario favors small λ, typically several orders of magnitude smaller than the ones considered in freeze-out. Hence, the particles never reach equilibrium but abundance increases until the interaction rate drops below the expansion rate after which the co-moving density remains constant. Analogously to freeze-out, this is called freeze-in and can be analyzed using similar methods. The main difference is regarding the initial state of the particles and the time at which the density starts to increase.

3.6.2 Comparing Analytical Calculations to Numerical Results

The results presented in fig. 3.2 shows the relation between $\langle\sigma v\rangle$ and m enforced by Ω_0. The relation between the two parameters was already predicted by the analytical approximation (3.22). This relation can be compared to relation (3.25) which was obtained by analyzing the figure. Evidently, the $\log\big(\langle\sigma v\rangle\big)$-term was not detected when investigating the figure. This can be explained by the variation in $\langle\sigma v\rangle$ being small when compared to the variations in m. Consequently, it is possible to treat the last term in relation (3.22) as a constant implying that it can be neglected. Thus, the analytical calculation is in accordance with the numerical results. Alternatively, it is possible to think of the contribution of the $\log\left(\langle\sigma v\rangle\right)$-term as negligible and therefore being hard to detect in the figure. Finally, it is crucial to emphasize that relation (3.25) is constrained by Ω_0 in conjunction with the model used and not by any physical relation between $\langle\sigma v\rangle$ and m or any model relating them to each other. The relation should therefore not be thought of as a necessary requirement for particles predicted by theory but rather as a limitation

on which particles are considered suitable, in the sense that the correct relic density is obtained according to our model.

As seen in fig. 3.3, the agreement between the analytical approximation (3.16) and numerical solutions to eq. (3.10) is relatively good. This implies that the analytical approximation is useful for estimating Y_∞ without having to solve the differential equation. It is worth mentioning that the range of λ spans several orders of magnitude which is of little physical relevance since it is indirectly constrained by the experimental values of Ω_0 in conjunction with $\langle\sigma v\rangle$ and m. For concreteness, a typical value is $\langle\sigma v\rangle = 1.8 \times 10^{-26}\,\mathrm{cm}^3\,\mathrm{s}^{-1}$ implying $m = 10^2\,\mathrm{GeV}$, as shown in fig. 3.2, which corresponds to $\lambda = 3.5 \times 10^{13}$. The large interval was solely used to show that the analytical approximation is valid even for values of the parameters $\langle\sigma v\rangle$ and m outside of the studied model. Moreover, the figure starts at $x_\mathrm{f} < 1$ and shows good results even though the analytical approximation was presented as being valid for $x_\mathrm{f} \gtrsim 3$. Further investigation showed that for $x_\mathrm{f} < 3$, the analytical approximation became more sensitive to c indicating that the approximation should be used with caution when x_f is small. However, it is important to remember that approximation (3.18) has been used to calculate x_f throughout this analysis which also introduces an error. This error is hard to quantify since x_f is a concept rather than an exact time, consequently, it lacks a strict definition.

3.6.3 Further remarks

Numerical calculations were used to analyze the error caused by some assumptions. As mentioned in section 3.1, it is assumed that the initial condition $Y(1) = Y_\mathrm{EQ}(1)$ is valid for freeze-out. It is possible to motivate this by solving eq. (3.10) to find Y_∞ with practically arbitrary initial conditions. As seen in fig. 3.4, all solutions falls into equilibrium before freeze-out. The upper and lower initial conditions are $Y(1) = Y_\mathrm{EQ}(1) \times 10^{\pm 3}$. The figure also shows that increasing values for λ leads to quicker regression toward equilibrium. It is also important to emphasize that the λ used are several orders of magnitude smaller than those encountered in common WIMP scenarios, any realistic λ would almost instantly return to equilibrium. Consequently, the assumption regarding the initial condition is valid.

Secondly, it has been assumed that Maxwell-Boltzmann statistics are valid when calculating the equilibrium distribution given by eq. (2.16). When using Fermi-Dirac or Bose-Einstein statistics instead, discrepancies are introduced, shown in fig. 3.5. It shows that the quantum mechanical effects have a small impact that is limited to early times when the particles were in equilibrium. Thus, since both the Fermi-Dirac and Bose-Einstein solution coincide with the Maxwell-Boltzmann solution before freeze-out, it is safe to neglect the differences as only the abundance at freeze-out affects the relic density.

Another major assumption is that all dark matter consists of only one type of particle. Mathematically this translates to $\Omega_\psi = \Omega_\mathrm{DM}$. Since there is very little knowledge of dark matter and its constituents, it is hard to determine whether the assumption is justified or not. This is only relevant when comparing calculated values to experimental data and does not affect the model unless the different kinds of dark matter particles are interacting. Hence, it is important to remember that the computations involving comparison with experimental data in this report needs to be revised if there exist several kinds of dark matter particles.

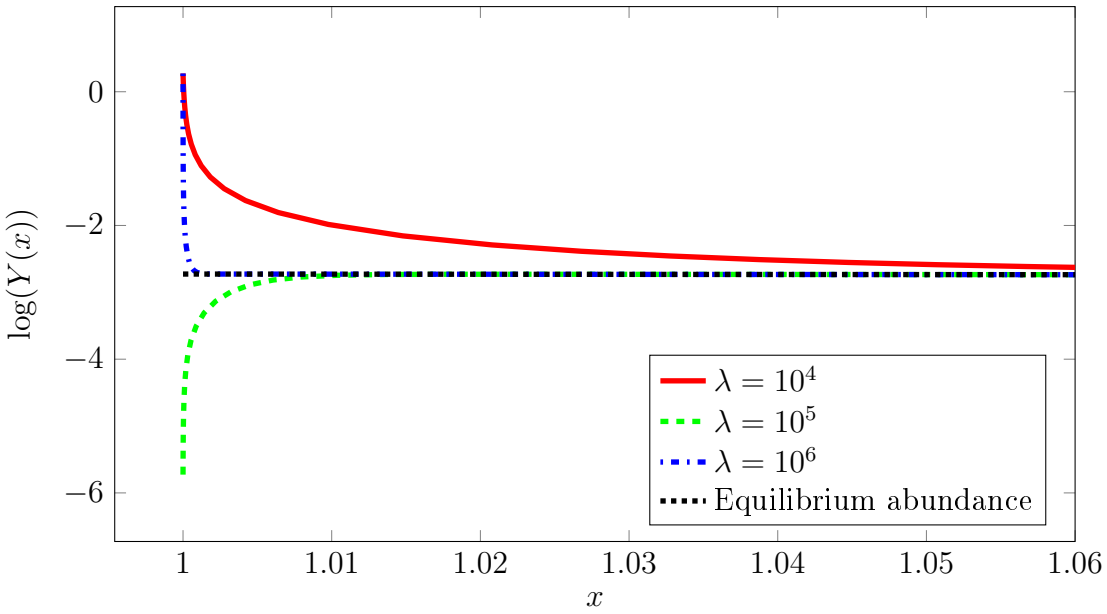

Figure 3.4: The initial condition is motivated by the solution quickly approaching equilibrium due to the high interaction rate. Large λ causes deviations to diminish quicker and vice versa, note that the λ used are very small in this context. The extreme initial conditions are $Y(1) = Y_{\text{EQ}}(1) \times 10^{\pm 3}$.

As mentioned in section 3.2, the only allowed interaction is self-annihilation. Interactions with ordinary matter has been neglected which is motivated by the very nature of dark matter. Furthermore, symmetry between ψ and $\bar{\psi}$ has been assumed, meaning that an equal number of both exists. This must not necessarily be the case and is therefore another uncertain assumption that has been made.

Finally, we can compare our results to typical theoretically predicted values for WIMPs. As described in section 2.4.3, one of the main reasons WIMPs are popular is because the predicted parameter values leads to the correct relic density. We approached this by choosing the mass interval to match popular candidates. Consequently, our calculated constraints are expected to meet the theoretically predicted values for $\langle \sigma v \rangle$. This can be verified by comparing our results with previous works, for example the paper by Steigman et al. [19]. In particular, fig. 3.2 can be compared to fig. 5 in their article. Our result is less accurate since the model used is simpler but it is still possible to tell that they are very similar.

3.6.4 Future Work

This report has implemented arguably the most simple non-trivial model for the Universe and the dark matter particles. Almost every assumption mentioned throughout this report can be studied more thoroughly. Some will prove to result in negligible errors, similar to the more detailed study of the effect of the initial condition, while others certainly are crucial to the final results. For example, further research should be done to investigate the possibility of different kinds of dark matter particles since it is highly likely to affect the results.

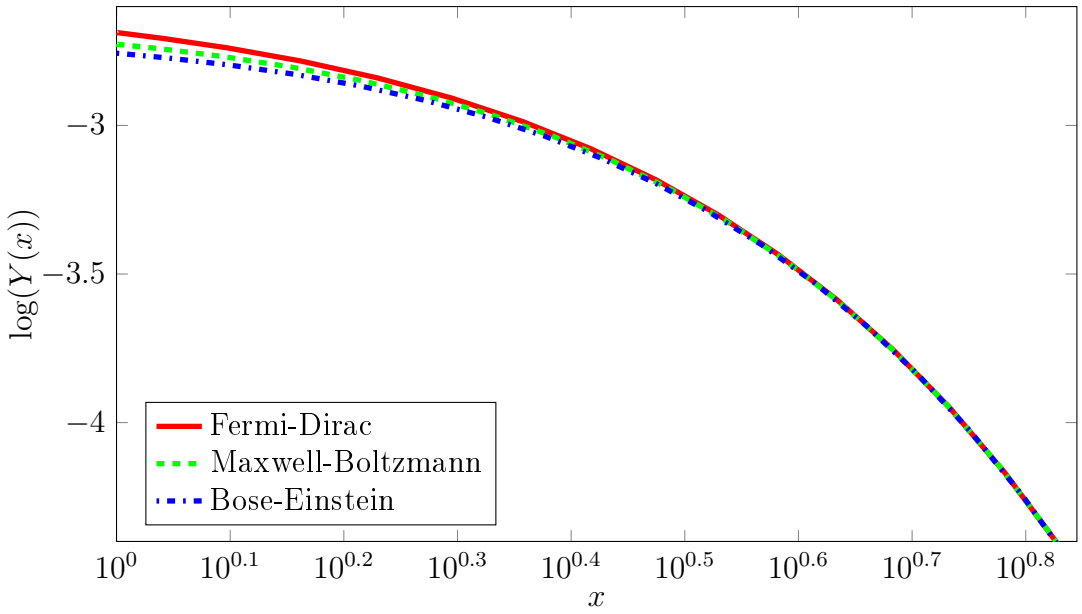

Figure 3.5: The figure shows the small differences between Fermi-Dirac, Bose-Einstein and Maxwell-Boltzmann statistics at early times. This shows that Maxwell-Boltzmann statistics may be used since all solutions coincide before freeze-out and, consequently, the relic abundance is the same regardless of distribution used.

Besides making a more accurate model, the current model can applied to other scenarios than just freeze-out. As previously mentioned, the freeze-in scenario relies on a similar mathematical framework but allows entirely different candidates since the physical processes are different. Some significant differences are that $\langle \sigma v \rangle$ is several orders of magnitude smaller than in a freeze-out scenario and the time of freeze-in is also several orders of magnitude smaller than x_{f}. Moreover, it is possible to investigate the evolution of particles at late times with slight modifications to the model presented in this report. This is of interest since observations could potentially measure Ω_{DM} at earlier times. The expected result is that $\Omega_{\mathrm{DM}} = \Omega_{\mathrm{DM},0}$ since the dark matter abundance is expected to be constant. However, this could still be used to determine "how constant" the density is at late times which theoretically could act as a constraint.

Chapter 4

Summary and Conclusions

The present study was designed to determine the evolution of the dark matter abundance in the Universe and to put constraints on the parameter space of an unknown dark matter particle. In the report we have developed the tools necessary to analyze the abundance of dark matter in our Universe. For the mathematical analysis, a thorough derivation of the Boltzmann equation for dark matter was made. Supposing that the dark matter is of particulate nature, we continued to develop a model where the dark matter is assumed to have been in equilibrium at some time, the freeze-out model.

For determining the dark matter relic abundance, the Boltzmann equation (3.10) is developed. It is then possible to give an approximate closed-form expression (3.16) for the relic abundance. Comparing with numerical solutions in fig. 3.1 shows that the approximate value is valid to an accuracy of 15 % in the relevant interval. The numerical solutions show that the abundance closely follows the equilibrium abundance initially. When the abundance starts to deviate from equilibrium it quickly stabilizes and becomes constant, allowing us to extrapolate that value to the present relic abundance. As expected, a larger cross section means that the dark matter abundance stays in equilibrium longer, leading to lower relic density since the equilibrium abundance decreases exponentially in x.

Using the recently measured value of $\Omega_{\mathrm{DM}} = 0.268$ to correlate the cross section and particle mass, we show that the allowed cross section seems to depend logarithmically on the particle mass. This result is also motivated by direct analysis of the Boltzmann equation. The dependance is shown in fig. 3.2 and makes evident that the relic abundance is very insensitive to the mass of the particle. In fact, in this model, the cross section can be determined to a very narrow interval. To yield the correct relic density, a particle in the freeze-out model should have a cross section

$$1.6\,\mathrm{cm}^3\,\mathrm{s}^{-1} < \langle \sigma v \rangle < 2.2\,\mathrm{cm}^3\,\mathrm{s}^{-1}, \tag{4.1}$$

an interval which may be augmented if considering a candidate with mass outside of the interval $10^1\,\mathrm{GeV} < m < 10^4\,\mathrm{GeV}$.

While these results do not directly answer the question of what dark matter actually consists of, they are a small step in determining where to look for particle dark matter. Some suggestions for further work has been made, for example analyzing the possibility of dark matter constituting of several kinds of particles. To sum up, more experimental research is required to actually find the particles and confirm the theory.

Bibliography

[1] Copernicus N., De revolutionibus orbium coelestium, Nuremberg, Holy Roman Empire of the German Nation; 1543, Latin.

[2] Freeman K., McNamara G., In Search of Dark Matter, Germany, Springer; 2006.

[3] Bergstrom L., Non-baryonic dark matter: Observational evidence and detection methods, Reports on Progress in Physics **63**, 793–841, 2005.

[4] Trimble V., Existence and nature of dark matter in the universe, Annual Review of Astronomy and Astrophysics **25**, 425–472, 1987.

[5] Ade P.A.R., Aghanim N., Armitage-Caplan C., Arnaud M., Ashdown M., Atrio-Barandela F., et al. Planck 2013 results. XVI. Cosmological parameters., 2013, arXiv:1303.5076v2 [astro-ph.CO]

[6] Abazajian K., Fuller G.M., Patel M., Sterile neutrino hot, warm, and cold dark matter, Phys. Rev. D **64**, 2001.

[7] Dodelson S., Modern Cosmology, 525 B Street San Diego (CA), Academic Press; 2003.

[8] Perlmutter S., Aldering G., Goldhaber G., Knop R.A., Nugent P., Castro P.G., et al., Measurements of Omega and Lambda from 42 High-Redshift Supernovae, Astrophys. J. **517**, 565, 1999.

[9] Scrimgeour M.I., Davis T., Blake C., James J.B., Poole G.B., Staveley-Smith L., et al. The WiggleZ Dark Energy Survey: the transition to large-scale cosmic homogeneity, Mon. Not. Roy. Astron. Soc. **425**, 116–134, 2012.

[10] Bertone G., Hooper D., Silk J., Particle Dark Matter: Evidence, Candidates and Constraints. Phys. Rept. **405**, 279–390, 2005.

[11] Friedmann A., Über die Krümmung des Raumes, Z. Phys. **10** (1), 377–386, 1922.

[12] Babcock H., The rotation of the Andromeda Nebula, Lick Observatory bulletin **498**, 1939.

[13] Kolb E.W., Turner M.S., The Early Universe, Redwood City (CA), Addison-Wesley; 1990.

[14] Koopmans L.V.E., Treu T., The Structure and Dynamics of Luminous and Dark Matter in the Early-Type Lens Galaxy of 0047-281 at $z = 0.485$, Astrophys. J. **583**, 606–615, 2003.

[15] Zwicky F., Die Rotverschiebung von extragalaktischen Nebeln, Helv. Phys. Acta **6**, 110–127, 1933, German.

[16] Bennett C.L., et al., Nine-Year Wilkinson Microwave Anisotropy Probe (WMAP) Obervations: Final Maps and Results, ApJS. **208**, 20B, 2013.

[17] Blennow M., Fernandez-Martínez E., Zaldívar B., Freeze-in through portals, 2013, arXiv:1309.7348 [hep-ph]

[18] Boltzmann L., Weitere Studien über das Wörmegleichgewicht unter Gasmolekülen, Sitzungsberichte Akad. Wiss., Vienna, part II **66**, 275–370, 1872, German.

[19] Steigman G., Dasgupta B., Beacom J.F., Precise Relic WIMP Abundance and its Impact on Searches for Dark Matter Annihilation, Phys. Rev. D **86**, 2012.